Ozone Production in Boreal Fire Smoke Plumes using observations from the Tropospheric Emission Spectrometer and the Ozone Monitoring Instrument

Sunita Verma[1], John Worden[1], Brad Pierce [2], Dylan B. A. Jones [3], Jassim Al-Saadi [4], Folkert Boersma[5], Kevin Bowman[1], Annmarie Eldering [1], Brendan Fisher[1], Line Jourdain[1], Susan Kulawik[1] and Helen Worden [1].

[1] Jet Propulsion Laboratory, California Institute of Technology, Pasadena, CA-91109, USA

2NOAA/NESDIS Advanced Satellite Products Branch, Madison, WI

3Universityof Toronto, Toronto, Ontario, Canada

4 NASA Langley Research Center, Hampton, VA 23681-0001

5 Harvard University, Cambridge, MA 02138

Abstract

We examine the photochemical processes governing the production of ozone in smoke from large Siberian fires that formed in July 2006 using co-located O_3 and CO profiles as measured by the Tropospheric Emission Spectrometer (TES) as well as NO_2 and aerosol optical depths as measured by the Ozone Monitoring Instrument (OMI). The Real-time Air Quality Model (RAQMS) is used to explain the observed variations of O_3. Enhanced levels of ozone up to 90 parts per billion (ppbv) are observed near and away from the Siberian fires (60^oN and 100^oE) when sunlight and NOx are available. We also observe significantly low O_3 amounts (less then 30 ppbv) in the smoke plume from Siberian fires in conjunction with optically thick aerosols. Despite this wide variance in observed ozone values, the mean ozone value for all observations of the smoke plume is close to background levels of approximately 55 ppbv in the free troposphere. Using RAQMS we show that optically thick aerosols in the smoke plume can substantially reduce the photochemical production of ozone and this can explain why the observed mean ozone amount for all plume observations is not much larger than background values of 55 ppbv. However, the anonymously low ozone amounts of 30 ppbv or less point towards other unresolved processes that reduce ozone below background levels in the plume.

1. Introduction

Long-range transport of smoke emissions from boreal fires can increase the atmospheric abundance of pollution over population centers. Prior studies [Wotawa and Trainer 2000; Forster et al. 2001] have shown, for example, that transport of emissions from the Canadian boreal fires can significantly increase atmospheric abundances of carbon monoxide (CO), aerosols, and ozone (O_3) over North American and European population centers. Bertschi and Jaffe [2005] showed, using satellite observations of aerosols and global aerosol transport model, that Siberian fire emissions were the primary source of three air pollution events off the coast of Washington State in 2003.

Boreal fires play an important role in the magnitude and inter-annual variability of tropospheric CO in the Northern Hemisphere [e.g., Novelli et al., 2003; Edwards et al., 2004; Kasischke et al., 2005, Pfister et al., 2005, Nedelec et al., 2005]. Several studies indicate that boreal fires can impact summertime O_3 over northwestern North America [Jaffe et al., 2004, Morris et al, 2006], the central North Atlantic [Lapina et al., 2006] and Europe [Simmonds et al., 2005]. The understanding of how boreal fires impact tropospheric O_3 is difficult, however because O_3 production in boreal fires is highly variable (Mauzerall et al., 1996, Lapina et al., 2006, Val Martin et al., 2006, Real et al., 2007). Real et al., [2007] reported significant O_3 variations in fire plumes depending upon the photochemical history of each plume. Val Martin et al., [2006] studied the impact of boreal fires in northern North America on the levels of black carbon (BC) aerosols, nitrogen oxides (NO_x) and O_3 downwind from North America. They noted that the boreal wildfire emissions significantly contributed to the NO_x and O_3 budgets in the lower free troposphere over the central North Atlantic during the summer of 2004.

Extensive fires burned in Siberia during the summer of 2006 as shown in Figure 1 which shows image from the Moderate Resolution Imaging Spectroradiometer (MODIS). As observed by both the Tropospheric Emission Spectrometer **(**TES) and the Ozone Monitoring Instrument (OMI), the plumes from these fires stretched across Siberia and the Pacific Ocean. The availability of satellite observations of CO, O_3, aerosols optical depth (AOD), and nitrogen dioxide (NO_2), for this period provides a valuable opportunity to evaluate our understanding of

factors controlling boreal fire emissions, their impact on atmospheric chemistry, and the transport of the ozone produced in this plume globally. This study examines O_3 produced and transported during July 2006 Siberian fire smoke plumes as observed from space-based observing platforms such as the Tropospheric Emission Spectrometer **(**TES) and the Ozone Monitoring Instrument (OMI) on the EOS-Aura satellite [Schoeberl, et al., 2006].

2. Satellite Observations used in analysis

2.1 TES

The TES instrument is an infrared Fourier transform spectrometer that measures the thermal emission of the Earth's surface and atmosphere over the spectral range 650-2250 cm^{-1}. It was designed to provide simultaneous vertical profile retrievals of tropospheric O_3, CO and other trace gases on a global basis [*Beer at al., 2001; Beer, 2006*]. The nadir footprint is 5.3 km across the spacecraft ground track and 8.5 km along track for the 16-detector average [*Beer et al.,* 2001]. TES has two basic science operating modes: Global Survey and Special Observations. Global Surveys are conducted every other day while special observations are taken as needed in between Global Surveys. We used global survey observations of TES O_3 and CO obtained between 20th July to 12th August 2006 with a nadir sampling of ~1.6° spacing along the ground track.

The analysis presented here utilizes TES version 003 data [*Osterman et al.,* 2006]. An overview of the TES retrieval algorithm and error estimation are discussed in *Bowman et al.* [2006] and the characterization of errors and vertical information for individual TES profiles are discussed in *Worden et al.* [2004] and *Kulawik et al.* [2006]. The vertical resolution of TES nadir O_3 retrievals is about 6 km for cloud-free scenes, with sensitivity to both the lower and upper troposphere [Worden et al., 2004; Bowman et al., 2006]. To date, TES tropospheric O_3 validation has been conducted through comparisons with ozonesondes [*Worden et al.,* 2007] and lidar *[Richards et al. 2007*]. These validation studies show that TES O_3 estimates are typically biased high in the upper troposphere by approximately 10%. Nassar et al. 2007 shows that TES O_3 is biased high by 3-10 ppb in the upper troposphere.

2.2 OMI

OMI is an ultraviolet and visible nadir solar backscatter imaging spectrograph which provides nearly global coverage in one day with a nadir spatial resolution of 13 x 24 km^2. OMI measures solar irradiance and Earth radiances in the wavelength range of 270 to 500 nm with a spectral resolution of about 0.5 nm. These radiances are used for estimating tropospheric column amounts of NO_2, HCHO, SO_2, AOD, as well as total O_3 amount [Levelt et al., 2006].

The analysis in this study utilizes OMI aerosol optical depth and NO_2 Level 2 version 3 data products. The OMI Level 2 geolocated geophysical parameters (O_3, NO_2, SO_2, BrO, HCHO, OClO, Aerosol, and Cloud) data products are at full instrument resolution, one orbit per file (http://disc.sci.gsfc.nasa.gov/data/datapool/OMI/). The basic algorithm for the retrieval of AOD and NO_2 from OMI data are described by Torres et al. (2002) and Boersma et al. (2007), Bucsela, et al. (2006), respectively. The NO_2 product was successfully validated with DC-8 aircraft NO_2 vertical profiles [Boersma et al., 2008].

3. Modeling tool used in analysis

3.1 Real-time Air Quality Modeling System (RAQMS)

Chemical and aerosol analyses from the Real time Air Quality modeling System (RAQMS) and ensemble wild fire trajectories are used to examine the different processes influencing the evolution of trace gases (e.g., O_3 and CO) within fire plumes during the 2006 Siberian boreal fires event. RAQMS is a unified (stratosphere/troposphere), online (meteorological, chemical, and aerosol) modeling system which has been developed for assimilating satellite observations of atmospheric chemical composition and providing real-time predictions of trace gas and aerosol distributions [Pierce et al., 2003, 2007; Kittaka et al., 2004, 2007]. The chemical formulation follows a family approach with partitioning based on photochemical equilibrium approximations. The Non Methane hydro-carbon (NMHC) chemical scheme is based on the carbon bond lumped-structure approach [Pierce et al., 2007]. Photolytic rates are calculated using the Fastj2 method [Bian et al., 2003]. The RAQMS aerosol model incorporates on-line aerosol modules from

GOCART [Chin et al., 2002, 2003] and a sulfate-nitrate-ammonium thermodynamic equilibrium model [Park et al., 2004]. Nine aerosol species (SO_4, NO_3, NH_4, hydrophobic organic carbon (OC), hydrophilic OC, hydrophobic BC, hydrophilic BC, dust, sea-salt) are transported. RAQMS biomass burning emissions use twice daily ecosystem/severity based emission estimates coupled with Moderate-resolution Imaging Spectroradiometer (MODIS) Rapid Response fire detections [Al-Saadi et al., 2007]. Total direct carbon emissions are calculated as the product of area burned and the ecosystem- and severity-specific carbon consumption estimates. Ecosystem dependent carbon consumption databases for three classes of fire severity (low, medium, high) are considered. Fire weather severity is estimated using the US Forest Service Haines Index, which considers atmospheric moisture and thermal stability [Haines, 1988]. Emissions of other species are determined by combining published emission ratios for different ecosystems [Cofer et al., 1991; Andreae and Merlet, 2001]. During the chemical and aerosol assimilation cycle the RAQMS meteorological forecasts are re-initialized from NOAA Global Forecasting System (GFS) analyses at 6 hour intervals.

The RAQMS chemical analysis used in the current study is from a retrospective 9-month (February-October, 2006) 2x2 degree assimilation that includes assimilation of cloud cleared OMI total column O_3 measurements and O_3 and CO profiles from TES nadir measurements. MODIS onboard the Aqua satellite (Remer et al. 2005, Davies et al. 2004) AOD was assimilated during the period from July 15th-July 31st to provide observational constraints for the investigation of the influences of aerosol loading on Siberian wild fire photochemistry. The MODIS AOD assimilation cycle was initialized from a Global Modeling and Assimilation Office (GMAO) aerosol forecast provided by Arlindo da Silva (NASA/GSFC). For the wild fire case studies only anthropogenic and biomass burning sources of carbonaceous aerosols were considered. Other aerosol species were passively advected. During the MODIS assimilation cycle, masses of all aerosol species were adjusted within each model layer based on the total AOD analysis increment and the relative contribution of each aerosol species to the total layer extinction. The MODIS AOD compares well with OMI AOD observations also used in this study with a correlation of approximately 0.7 between the two data sets but with OMI AOD showing slightly higher values than MODIS of about 0.2 AOD [Ahn *et al.*, 2006].

4. Methodology

During mid-July 2006, multiple forest fires were recorded across the central Siberian Plateau between the north-flowing Lena River and Lake Baikal along 95^{o}E longitude and 60^{o}N latitude (http://earthobservatory.nasa.gov/NaturalHazards/natural_hazards_v2.php3?img_id=13728). The Spatial distribution of the Siberian fires detected by MODIS during the period from 20th July to 26 July 2006 is shown in Fig. 1. The substantial fire hotspots located over Siberia from the MODIS fire-counts data between 55°N and 70°N are also shown in Figure 2 (marked as red) on 24th July 2006, which was the day of the peak Siberian wildfire emissions, as shown by MODIS fire-counts (Davies et al. 2004).

In order to examine the production of O_3 within the smoke plumes from these fires we first needed to identify the plume signature. TES and OMI observations from mid-July to mid August of 2006 were used. TES measurements with CO abundances greater than 120 ppb (e.g., Wolfy et al. 1992; Mauzerall et al. 1996) were identified as potentially impacted by upwind boreal fires. Co-located AOD from OMI were used as corroborating evidence. Images from MODIS were acquired during this period to compare with the satellite outputs as further corroborating evidence. We used backward trajectories from these observations of enhanced CO and aerosols to the fire source as well as forward trajectories from the fire source using both the FLEXPART model (Stohl et al., 1998) and RAQMS to ensure that the observed air parcels came from the Siberian fires of interest.

5. Discussions

5.1 Siberian Boreal Fire Emissions

The MODIS data revealed intense fire activity in the Siberian region during July 2006, near 95°E and 65°N as shown in Figures 1 and 2 (marked as red). Figure 2a shows the FLEXPART 10-day forward trajectories from this fire starting on July 24th, 2006. The light blue lines represent the forward trajectories for a plume starting from a TES orbit around 98°E and 62°N with altitude levels between 0 and 15 km. Figures 2b, c, and d shows the FLEXPART 5-day backward

trajectories (light blue lines) starting from a TES track location (shown as orange), corresponding to Figures 3, 4, and 6, respectively. The back trajectories in Figures 2b, c and d suggests that air sampled on the selected TES orbits is mainly from the Siberian fires as the trajectories show significant re-circulation in and around the fire source. The forward trajectories in Figure 2a indicate large plumes of smoke transported from northeastern Siberia to across the Pacific during late July, providing opportunities for many observations of the plume by TES and OMI.

5.2 TES and OMI observations for Siberian Smoke Plume

Because the smoke from the fires of interest travels eastward and the Aura satellite travels along a polar orbit there are many opportunities to observe cross-section of the fire plumes. We first show four examples showing vertical cross-sections of CO and O_3 values across fire plumes. The average CO and O_3 mixing ratios is also presented along these vertical cross-sections. As discussed earlier, in order to ensure that the observed air parcels are only related to smoke from the fires, the CO values from each observation are averaged together over the pressure (>400hPa) range for which CO values are larger than 120 ppbv. The ozone values are also averaged using similar criteria.

Figure 3a shows CO and O_3 profiles from TES on July 24th 2007 near the Siberian fire source (100-130E). The location of the Siberian fires are observed by MODIS to be approximately between 90°-110°E and 60°-70°N (Fig. 1&2). The vertical profiles of CO in Fig. 3a shows values ranging from background levels (~ 80 ppb) to enhanced levels (between 120 and 250 ppb). Back trajectories from the regions of high CO (Figure 2b) indicate that observed air parcels have re-circulated in and around the fire and therefore indicate the high CO is related to the fire emissions.

The vertical resolution of the TES ozone and CO estimates is approximately 6 km (Worden et al., 2006). However, it is appropriate to show these vertical profiles because the plume height depends on altitude and the sensitivity of the estimates depend on altitude. The sensitivity of the TES estimates are indicated by the diagonal of the averaging kernel matrices shown to the right of the CO and O_3 estimates. The diagonal of the averaging kernel matrix is

the sensitivity of the O_3 or CO estimate at the indicated pressure level to the actual amount of the species at the same pressure level. The greatest sensitivity of the CO and O_3 estimates is in the free troposphere between 400 hPa and 800 hPa. Peak values of the O_3 and CO averaging kernel diagonals correspond to peak values of O_3 and CO, and the largest variations of O_3 relative to background values of approximately 55 ppbv in the free troposphere. Consequently it is reasonable to assume that observed variations in O_3 and CO amounts in the free troposphere are at similar altitudes.

Fig. 3b shows aerosol optical depths as observed by OMI between 100 and 130 East degrees longitude and 50 and 75 North degrees latitude. The TES orbit track is also shown as a red curve over AOD values and the location of the TES observations are shown as diamonds overlaying the orbit track. The aerosols provide corroborating evidence that the observed air parcel interacted with the boreal fire plume. In fact, the largest values of AOD between 100-110^{o}E and 60–70^{o}N correspond to the fire locations as seen by the MODIS fire count data in Figure 1. Back trajectories from the locations of the TES observations (Figure 2b) indicate that the air parcels observed by TES had intersected the location of the fire approximately three days earlier. Enhanced O_3 is observed anywhere from 50^o N to 74^o N. NO_2 values of approximately 2 x10^{15} molec/cm^2 and relatively low AOD (AOD < 0.5) as seen in Fig. 3b, indicate the availability of O_3 pre-cursors and sunlight for photochemical production of O_3.

In order to better examine O_3 and CO variations within the plume we next average the CO values over those altitudes where CO is larger than 120 ppbv and the diagonal of the averaging kernel is larger than 0.05 and the sum of the diagonals (also known as the degrees of freedom for signal or DOFS) is larger than 0.5 for CO in the troposphere. The O_3 concentrations averaged over these same altitudes are shown in Figure 3c for observations that meet the above criteria. The total error estimates, calculated using the total error for each profile, averaged over the selected altitudes (Worden et al., 2006), is also shown. We find the total error for these averaged quantities are about 8-12% for O_3 and 6-10% for CO; these uncertainties are sufficient for resolving the observed O_3 and CO variations. For this plume cross section, we observe values ranging from 130 to 180 ppbv for CO and approximately 35 to 90 ppbv for O_3. There appears to be no correlation between the O_3 and CO amounts.

These same quantities are shown in Figure 4a for a region further away from the fire (approximately 50 degrees in Longitude) and at a later date (July 31st 2007). Enhanced levels of CO and AOD (AOD > 0.1) as well as back trajectories (Figure 2c) indicate the enhanced CO levels are due to the Siberian fire emissions. As seen in Figure 4c, enhanced O_3 of up to 70 ppbv is observed in regions where CO is moderately enhanced (between 120 and 200 ppb) and AOD is moderately enhanced (AOD ~ 0.5) along with the availability of NO_2. However, there are also a couple of observations with low ozone values which likely indicate that different parts of this large plume, covering up to 15 degrees in latitude, have different chemical histories. We explore these low ozone values next.

In contrast to the ozone shown in Figures 3 and 4, Figures 5a and 6a show cross-sections of the fire plume where O_3 is low relative to background values of approximately 55 ppb in the free troposphere. Figure 5a and 5b shows CO, O_3, AOD and NO_2, respectively directly over the region where the fires are burning on 24th July 2006. CO is observed with values exceeding 300 ppb (with the color scale on the top left panel saturating at 200 ppb) and the aerosol optical depth exceeding 4. NO_2 is observed with values ranging between $1x10^{15-}$ - $2 x10^{15}$ molec/cm^2. Ozone values ranging from 30 ppbv to 65 ppbv are observed. The lower ozone values occur in regions where AOD is optically thick (>3). Note that the high AOD values do not affect the TES estimates of CO and O_3 because thermal infrared radiation is not absorbed much by aerosols produced in fire (Kirchstetter et al. 2004).

This behavior of low O_3 within a plume with significant aerosol optical depth and significantly enhanced CO amounts (greater the 200 ppb) is also observed (Figure 6a) four days later (on 28 July 2008) for a plume that is 40 degrees away from the fire source at approximately 100°E. In both, the July 24th and 28th cases there is significant variation of O_3 across the plume, with low O_3 usually occurring in plume cross-sections with high AOD (AOD > 3) (Fig. 6b). Because this behavior is observed both over and away from the fire, where temperature conditions are expected to be different, we do not believe that incorrect estimates of temperature will affect these O_3 retrieval results.

To examine these relationships further we compute these same values as shown in Figures 4c through 8c for approximately 30 plume cross-sections of mid-July to mid-August 2006 where the air sampled originated from the Siberian smoke plumes. The mean O_3 and CO is computed for each cross-section along with the root-mean-square of the O_3 variability across the plume. These values are shown for these cross-sections in Figure 7. The symbols in Figure 7 are the mean values of CO and O_3 in the plume cross-section and the bars show the RMS of the O_3 in the cross-section. We observe that O_3 can vary significantly, with values ranging from 20 ppbv to 90 ppbv for a wide range of CO values. Despite this large variance, the mean O_3 for all observations is about the same as the background value of about 55 ppbv observed at similar latitudes but without enhanced CO. This suggests that while enhanced O_3 abundances are produced in this boreal fire plume, the average net O_3 production in the plume is small which is consistent with prior observations of aged O_3 plumes using tower and aircraft observations (Real et al. 2007, Mauzerall et al. 1996, Val Martin et al. 2006).

5.3 RAQMS Analysis

The chemical evolution of the Siberian boreal fires is further explored by sampling the RAQMS chemical analysis along the ensemble fire trajectories to understand the different processes and time evolution of trace gases within the plumes, with a particular focus on the evolution of O_3 and CO under different aerosol loadings. To investigate the impact of aerosols on O_3 production rates within the wild fire plumes we conducted two simulations, one with and one without BC and OC aerosols in the photolysis calculations.

5.3.1 Forward trajectory simulations

5.3.1.1 RAQMS Chemistry Run Without Aerosols

Figure 8 represent results from a photochemical calculation of O_3 in the RAQMS model in which an ensemble of 10-day forward trajectories samples the model output starting on July 24th 2006 for Siberia at 100E, 60N location. This run was conducted for the chemistry only simulation from RAQMS, that is, without aerosols in the photolysis calculations. Based on the RAQMS wild-fire emission estimates, this time period is associated with the highest wild fire

emission rates for this Siberian fire. The time evolution of O_3, CO concentrations, NO_y (or NO_x per day) and net O_3 production rates (Production-Loss) is shown in Fig. 8 along the smoke plume from this 10 day forward trajectory run. The time histories for each ensemble member (dots) and ensemble mean (solid line) are shown. There is a large increase in O_3 concentrations in the fresh part of plume (ensemble mean goes from 80 to 130 ppb within the first 24 hours). This increase in O_3 concentrations is due to large daytime net production of O_3 (exceeding 120ppb/day 24hrs after the start of the trajectory calculation) associated with high NO_2 mixing ratios (net NO_2 emissions reach 34 ppb/day). The peak O_3 mixing ratios within the fresh wild fire plume in the model of nearly 140 ppb is significantly larger than observed by TES which shows peak values of 90 ppb in the vicinity of the wild fire plume (see Figure 3a).

5.3.1.2 RAQMS Sensitivity run: Aerosols Impact on Ozone production: High Aerosol Loading

A second ensemble of 10-day forward trajectories starting on July 24th 2006 Siberia is shown in Fig. 9 for a RAQMS chemistry simulation that also includes BC and OC aerosols in the photolysis calculations. In contrast to the chemistry only simulation, the RAQMS model including aerosols shows only slight increases in O_3 concentrations in the fresh part of the plume with the ensemble mean ranging from 60-70 ppb within the first 24hrs. This slight increase in O_3 concentrations is due to enhanced daytime net O_3 production (which was about 29 ppb/day at 24hrs). This represents a four-fold decrease in net O_3 production relative to the model simulation without aerosols and suggests that optically thick aerosols (AOD > 3) during the most intense phase of the Siberian wild fire event significantly inhibit photolysis and hence greatly modifies the O_3 production; this conclusion is consistent with the results of Real et al.(2007) who also discussed the effects of aerosols on reduced O_3 production. However, neither simulation is able to replicate the low O_3 observations of about 30 - 40 ppb observed by TES, which may be due to other chemical processes at the fire source such as aerosol surface chemistry (e.g Val Martin *et al.*, 2006; Real et al. 2007) or O_3 destruction due to the titration of NO_x within the fresh plume (Crutzen and Bruhl, 2001).

6. Discussion and Conclusions

Ozone production in the July 2006 Siberian boreal fire is examined using synchronous tropospheric observations of O_3 and CO from TES and observations of aerosol optical depth and NO_2 column abundances from OMI. These observations show that Siberian biomass burning emissions can produce elevated O_3 within the fire plume. However, O_3 abundances in the Siberian boreal forest fire plumes are highly variable, with some plumes showing O_3 enhancements of up to 90 ppb and others showing no enhancement or even O_3 depletion, with abundances of 30 ppb, much lower than background tropospheric values of about 55 ppb.

We investigated the impact of aerosols on O_3 production rates within the wild fire plumes using the RAQMS model. In the absence of aerosols, the RAQMS model predicts up to 120 ppb of O_3 in the fire plume. Accounting for the presence of optically thick aerosols by assimilating in the model AOD data from the MODIS instrument reduced the photolysis rates in the model. As a result, in regions with optically thick aerosols, the model predicted a significant decrease in the net production of O_3, from about 120 ppb/day to 30 ppb/day within 24hrs of the plume emission. O_3 concentrations in the model simulation with the assimilated AOD were approximately 60 ppb which is consistent with the mean ozone for all plume observations. Reduced photolysis due to aerosols, and, by the same reasoning, clouds, could therefore explain the lack of enhanced O_3 levels seen in the boreal fire plume produced by the Siberian fires. However, the anomalously low O_3 abundances of 30 ppb are also observed indicating that additional O_3 loss mechanisms, such as NO_2 titration or aerosol surface chemistry, could be important in determining the observed O_3 abundances. Combining these satellite observations with in situ observations of O_3 and its pre-cursors such as those from the 2008 Arctic Research of the Composition of the Troposphere from Aircraft and Satellites (ARCTAS: http://www.espo.nasa.gov/arctas/) aircraft campaign should greatly improve understanding of ozone production and loss mechanisms in boreal fire smoke plumes and their impact on global atmospheric composition.

Acknowledgement

We would like to thank Jennifer Logan and Daniel Jacob for there helpful suggestions in the analysis of this data. The work described here is performed at the Jet Propulsion Laboratory, California Institute of Technology under contracts from the National Aeronautics and Space

Administration. DBAJ was funded by the Natural Sciences and Engineering Council of Canada and the Canadian Foundation for Climate and Atmospheric Sciences. The views, opinions, and findings contained in this report are those of the author(s) and should not be construed as an official National Oceanic and Atmospheric Administration or U.S. Government position, policy, or decision.

References

Ahn, C., O. Torres, and P. K. Bhartia (2008), Comparison of Ozone Monitoring Instrument UV Aerosol Products with Aqua/Moderate Resolution Imaging Spectroradiometer and Multiangle Imaging Spectroradiometer observations in 2006, J. Geophys. Res., 113, D16S27, doi:10.1029/2007JD008832.

Andreae, M. O. and P. Merlet (2001), Emission of trace gases and aerosols from biomass burning. Global Biogeochemical Cycles, 15: 955-966, 2000GB001382.

Al-Saadi, J. et al. (2007), Global Near-Real-Time Estimates of Biomass Burning Emissions using Satellite Active Fire Detections, submitted, JARS.

Beer, R., T. A. Glavich, and D. M. Rider (2001), Tropospheric emission spectrometer for the Earth Observing System's Aura satellite, Appl. Opt., 40, 2356–2367.

Beer, R. (2006), TES on the Aura Mission: Scientific Objectives, Measurements and Analysis Overview, IEEE Transactions on Geoscience and Remote Sensing, 44, 1102-1105.

Bertschi, I. T., and D. A. Jaffe (2005), Long-range transport of ozone, carbon monoxide, and aerosols to the NE Pacific troposphere during the summer of 2003: Observations of smoke plumes from Asian boreal fires, J. Geophys. Res., 110, D05303,doi:10.1029/2004JD005135.

Bian, H., M. Prather, and T. Takemura (2003), Tropospheric aerosol impacts on trace-gas budgets through photolysis, J. Geophys. Res., 108, 4242, doi:10.1029/2002JD002743.

Boersma, K. F., E. J. Bucsela, E. J. Brinksma, and J. F. Gleason (2002) NO2 in OMI Algorithm Theoretical Basis Document, vol. 4, OMI Trace Gas Algorithms, ATBD-OMI-04, Version 2.0, edited by K. Chance, pp. 13-36, NASA Distrib. Active Arch. Cent., Greenbelt, Md., Aug., 2002.

Boersma, K. F., H. J. Eskes, J. P. Veefkind, E. J. Brinksma, R. J. van der A, M. Sneep, G. H. J. van den Oord, P. F. Levelt, P. Stammes, J. F. Gleason, and E. J. Bucsela (2007), Near-real time retrieval of tropospheric NO_2 from OMI, *Atmos. Chem. Phys., 7*, 2103-2118.

Boersma, K. F., D. J. Jacob, E. J. Bucsela, A. E. Perring, R. Dirksen, R. J. van der A, R. M. Yantosca, R. J. Park, M. O. Wenig, T. H. Bertram, and R. C. Cohen (2008), Validation of OMI tropospheric NO_2 observations during INTEX-B and application to constrain NO_x emissions over the eastern United States and Mexico, *Atmos. Environ.*, doi:10.1026/j.atmosenv.2008.02.004, in press.

Bowman, K. W., et al. (2006), Tropospheric emission spectrometer: Retrieval method and error analysis, IEEE Trans. Geosci. Remote. Sens., 44, 1297–1307.

Bucsela, E. J., E. A. Celarier, M. O. Wenig, J. F. Gleason, J. P. Veefkind, K. F. Boersma, and E. J. Brinksma (2006), Algorithm for NO2 vertical column retrieval from the Ozone Monitoring Instrument, IEEE Trans. Geo. Rem. Sens., 44(5), 1245-1258, Special Issue on the EOS Aura Mission.

Chin, M. et al. (2002), Tropospheric aerosol optical thickness from the GOCART model and comparisons with satellite and sunphotometer measurements, J. Atmos. Sci., 59, 461-483.

Chin, M. et al. (2003), A global aerosol model forecast for the ACE-Asia field experiment, J. Geophys. Res., 108(D23), 8654, doi:10.1029/2003JD003642.

Cofer, W.R. III, J. S. Levine, E. L. Winstead, and B. J. Stocks (1991), Trace gas and particulate emissions from biomass burning in temperate ecosystems, in Global Biomass Burning: Atmospheric, Climatic, and Biospheric Implications, J.S. Levine (Ed.), MIT Press, Cambridge, Mass., 203-208.

Crutzen, P. J. and C. Bruhl (2001), Catalysis by NO_x as the Main Cause of the Spring to Fall Stratospheric Ozone Decline in the Northern Hemisphere J. Phys. Chem. A, 105, 9, 10.1021/jp001984h, 1579 – 1582.

Davies, D., S. Kumar, and J. Descloitres (2004), Global fire monitoring using MODIS near-real-time satellite data. GIM International, 18(4):41.

Edwards, D. P., et al. (2004), Observations of carbon monoxide and aerosols from the Terra satellite: Northern Hemisphere variability, J. Geophys. Res., 109, D24202, doi:10.1029/2004JD004727.

Forster, C., U. Wandinger, G. Wotawa, P. James, I. Mattis, D. Althausen, P. Simmonds, S. O'Doherty, C. Kleefeld, S. G. Jennings, J. Schneider, T. Trickl, S. Kreipl, H. Jäger, and A. Stohl (2001): Transport of boreal forest fire emissions from Canada to Europe . *J. Geophys. Res.***106**, 22,887-22,906.

Haines, D.A. (1988), A lower atmosphere severity index for wildland fires. National Weather Digest, 13, 23-27.

Jaffe, D., I. Bertschi, L. Jaegle, P. Novelli, J. S. Reid, H. Tanimoto, R. Vingarzan, and D. L. Westphal (2004) Long-range transport of Siberian biomass burning emissions and impact on surface ozone in western North America, Geophys. Res. Lett., 31, L16106, doi:10.1029/2004GL020093.

Kasischke, E. S., E. J. Hyer, P. C. Novelli, L. P. Bruhwiler, N. H. F. French, A; I. Sukhinin, J. H. Hewson, and B. J. Stocks (2005), Influence of boreal fire emissions on Northern Hemisphere atmospheric carbon and carbon monoxide, Global Biogeochem. Cycles, 19 (1), GB1012, 10.1029/2004GB002300.

Kirchstetter, T. W., et al. (2004), Evidence that the spectral dependence of light absorption by aerosols is affected by organic carbon, Journal of Geophysical Research-Atmospheres, 109, -.
Kittaka, C. et al. (2004), A three-dimensional regional modeling study of the impact of clouds on sulfate distributions during TRACE-P, J. Geophys. Res., 109, D15S11, doi:10.1029/2003JD004353.

Kulawik, S. S., G. Osterman, D. B. A. Jones, and K. W. Bowman (2006), Calculation of altitude-dependent Tikhonov constraints for TES nadir retrievals, IEEE Trans. Geosci. Remote Sens., 44, 1334– 1342.

Kulawik, S. S., et al. (2006), Implementation of cloud retrievals for Tropospheric Emission Spectrometer (TES) atmospheric retrievals: part 1. Description and characterization of errors on trace gas retrievals, *Journal of Geophysical Research-Atmospheres*, *111*, -.

Lapina, K., R. E. Honrath, R. C. Owen, Val Martin, and G., Pfister (2006)., Evidence of significant large-scale impacts of boreal fires on ozone levels in the midlatitude Northern Hemisphere free troposphere, Geophys. Res. Lett., 33, L18015, doi:10.1029/2006GL025878.

Levelt, P. F., et al. (2006), Science objectives of the Ozone Monitoring Instrument, IEEE Trans. Geophys. Remote Sens., 44(5), 1199–1208.

Mauzerall, D. L., et al. (1996), Origin of tropospheric ozone at remote high northern latitudes in summer, Journal of Geophysical Research-Atmospheres, 101, 4175-4188.

Morris, G.A., S. Hersey, A.M. Thompson, O.R. Cooper, A. Stohl, P.R. Colarco, W.W. McMillan, J. Warner, B.J. Johnson, J.C. Witte, T.L. Kucsera, D.E. Larko, and S.J. Oltmans, Alaskan and Canadian forest fires exacerbate ozone pollution over Houston, Texas, on 19 and 20 July 2004, J. Geophys. Res., 111, D24S03, doi:10.1029/2006JD007090, 2006.

Nassar, R., J. A. Logan, H. M. Worden, et al. (2007), Validation of Tropospheric Emission Spectrometer (TES) Nadir Ozone Profiles Using Ozonesonde Measurements, J. Geophys. Res., doi:10.1029/2007JD008819, in press.

Nedelec, P., V. Thouret, J. Brioude, B. Sauvage, J.-P. Cammas, and A. Stohl (2005), Extreme CO concentrations in the upper troposphere over northeast Asia in June 2003 from the in situ MOZAIC aircraft data, *Geophys. Res. Lett.*, *32*, L14807, doi:10.1029/2005GL023141.

Novelli, P. C., K. A. Masarie, P. M. Lang, B. D. Hall, R. C. Myers, and J. W. Elkins (2003), Reanalysis of tropospheric CO trends: Effects of the 1997–1998 wildfires, J. Geophys. Res., 108(D15), 4464, doi:10.1029/2002JD003031.

Osterman, G., et al. (2005), Tropospheric emission spectrometer (TES) validation report, version 1.00, D33192, Jet Propul. Lab., Pasadena, Calif. (Available at http://tes.jpl.nasa.gov/docsLinks/documents.cfm)

Park, R. J. et al. (2004), Natural and transboundary pollution influences on sulfate-nitrate-ammonium aerosols in the United States: Implications for policy, J. Geophys. Res., 2004, 109, D15204, doi:10.1029/2003JD004473.

Pfister, G., P. G. Hess, L. K. Emmons, J.-F. Lamarque, C. Wiedinmyer, D. P. Edwards, G. Pétron, J. C. Gille, and G. W. Sachse. (2004), Quantifying CO emissions from the 2004 Alaskan wildfires using MOPITT CO data, GRL, 32.

Pierce, R. B. et al. (2003), Regional Air Quality Modeling System (RAQMS) predictions of the tropospheric ozone budget over east Asia, J. Geophys. Res. 108, 8825, doi:10.1029/2002JD003176.

Pierce, R. B., et al. (2007), Chemical data assimilation estimates of continental US ozone and nitrogen budgets during the Intercontinental Chemical Transport Experiment-North America. J. Geophys. Res. doi: 10.1029/2006JD007722.
Real, E., et al. (2007), Processes influencing ozone levels in Alaskan forest fire plumes during long-range transport over the North Atlantic, J. Geophys. Res., 112, D10S41, doi:10.1029/2006JD007576.

Remer, L. A., Y. J. Kaufman, D. Tanré, S. Mattoo, D. A. Chu, J. V. Martins, R.-R. Li, C. Ichoku, R. C. Levy, R. G. Kleidman, T. F. Eck, and E.; Vermote (2005), The MODIS aerosol algorithm, products and validation. J. Atmos. Sci., 62, 947-973.

Richards, N. A. D., Q. B. Li, G. B. Osterman, E. V. Browell, M. Avery, and K. W. Bowman (2007) Validation of TES tropospheric ozone profiles with airborne LIDAR observations, J. Geophys. Res., submitted.

Rodgers, C. D. (2000), *Inverse methods for atmospheric sounding : theory and practice*, xvi, 238 p. pp., World Scientific, Singapore ; London.

Schoeberl, M. R., et al. (2006), IEEE Transactions on Geoscience and Remote Sensing 44 (5), 1066-1074.

Simmonds, P. G., A. J. Manning, R. G. Derwent, P. Ciais, M. Ramonet, V. Kazan, and D. Ryall (2005), A burning question: Can recent growth rate anomalies in the greenhouse gases be attributed to large-scale biomass burning events?, Atmos. Environ., 39, 2513– 2517.

Stohl, A., M. Hittenberger, and G. Wotawa (1998): Validation of the Lagrangian particle dispersion model FLEXPART against large scale tracer experiments. Atmos. Environ. 24, 4245-4264.

Torres, O., R. Decae, J. P. Veefkind, and G. de Leeuw (2002), OMI Aerosol Retrieval Algorithm, in OMI Algorithm Theoretical Basis Document, vol. 3, Clouds, Aerosols, and Surface Irradiance, ATBD-OMI-03, Version 2.0, edited by P. Stammes, pp. 13-36, NASA Distrib. Active Arch. Cent., Greenbelt, Md., Aug.

Val Martin, M., R. Honrath, R. C. Owen, G. Pfister, P. Fialho and F. Barata (2006), Significant enhancements of nitrogen oxides, ozone and aerosol black carbon in the North Atlantic lower free troposphere resulting from North American boreal wildfires, J. Geophys. Res., 111, D23S60, doi:10.1029/2006JD007530.

Wofsy, S.C., et al. (1992), Atmospheric chemistry in the arctic and subarctic: influence of natural fires, industrial emissions, and stratospheric inputs, J. Geophys. Res., 97, 16731-16746.

Worden, H. M., et al. (2007), Comparisons of Tropospheric Emission Spectrometer (TES) ozone profiles to ozonesondes: Methods and initial results, J. Geophys. Res., 112, D03309, doi:10.1029/2006JD007258.

Worden, J., S. S. Kulawik, M. W. Shephard, S. A. Clough, H. Worden, K. Bowman, and A. Goldman (2004), Predicted errors of tropospheric emission spectrometer nadir retrievals from spectral window selection, J. Geophys. Res., 109, D09308, doi:10.1029/2004JD004522.

Wotowa, G., and Trainer M., (2000), The Influence of Canadian Forest Fires on Pollutant Concentrations in the United States, Science, Vol. 288, 5464, 324-328.

Figure captions

Figure 1: Spatial distribution of the Siberian fires detected by MODIS during the period 20–26th July 2006.

Figure 2: The 10 day (a) forward trajectories (blue lines) from peak Siberian wildfire emissions for a plume starting around 98^{o}E and 62^{o}N on July 24th, 2006. Five day backward (blue lines) trajectories in (b), (c) and (d) starting from a TES track (shown as orange), corresponds to figures 3, 4, and 6, respectively. The trajectories represent the five different sets of latitude and longitudes pairs over the TES overpass and altitude levels between 0 and 15 km. Locations shown in red (marked as crosses) indicate the MODIS fire retrievals on 24th July 2006. The orbit tracks correspond to TES measurement locations chosen as examples in this study, as shown in Figures 4b, 6b, 3b, and 5b, respectively starting from west to east.

Figure 3: TES (a) CO, O_3 (left column) and Averaging Kernel (AK) diagonals (right column), (b) AOD and NO_2 tropospheric column amounts as observed from OMI, (c) Latitudinal variations of CO and O_3 mixing ratios averaged for CO > 120ppb and pressure > 400hPa for the plume values near the Siberian fires at 100°E-130°E on 24th July 2006. Overlaying the AOD and NO_2 (b) is the TES orbit track (red curve) with the locations of the TES observations indicated by diamonds.

Figure 4: Same as Figure 3 but for the plume away from the Siberian fires at 135°E-170°E, on 31st July 2006.

Figure 5: Same as Figure 3 but for the plume near the Siberian fires at 80°E-110°E, on 24th July 2006.

Figure 6: Same as Figure 3 but for the plume away from the Siberian fires at 130°E–160°E, on 28th July 2006.

Figure 7: Scatter plot for CO and O_3 mixing ratios for all plume observations averaged for the Siberian fire period (mid-July to mid-August, 2006).

Figure 8: 10 day forward trajectory simulation without aerosols initialized with 24th July 2006 upwind data and daily fire emissions (Tg/day) from real time MODIS fire counts at Siberia showing time evolution of O_3, CO concentrations, NO_y and O_3 production rates.

Figure 9: Same as Figure 8 but with aerosols.

(a)

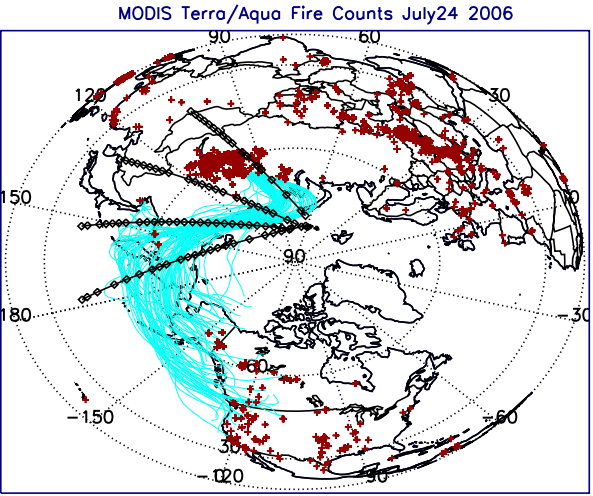
MODIS Terra/Aqua Fire Counts July24 2006
90
60
120
30
150
90
180
-30
-150
-60
30
-120
-90

(b)

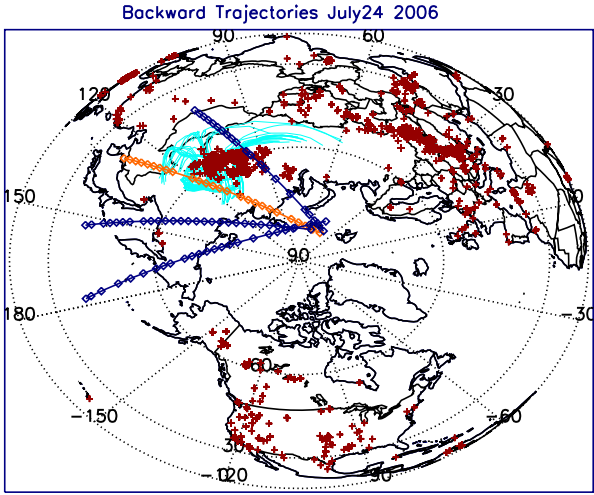
Backward Trajectories July24 2006
90
60
120
30
150
90
180
-30
-150
-60
30
-120
-90

(c)

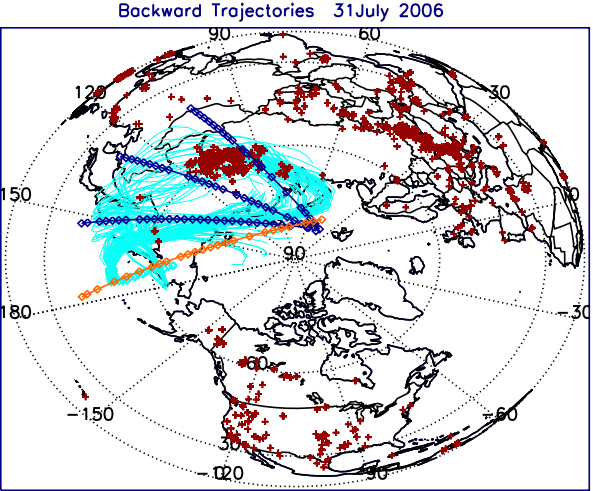
Backward Trajectories 31July 2006
90
60
120
30
150
90
180
-30
-150
-60
30
-120
-90

(d)

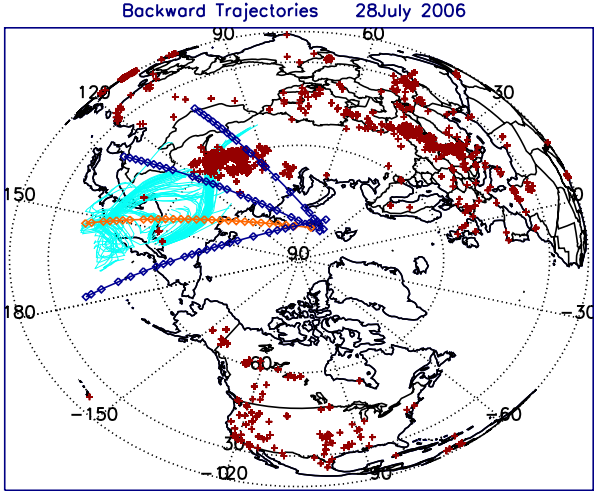
Backward Trajectories 28July 2006
90
60
120
30
150
90
180
-30
-150
-60
30
-120
-90

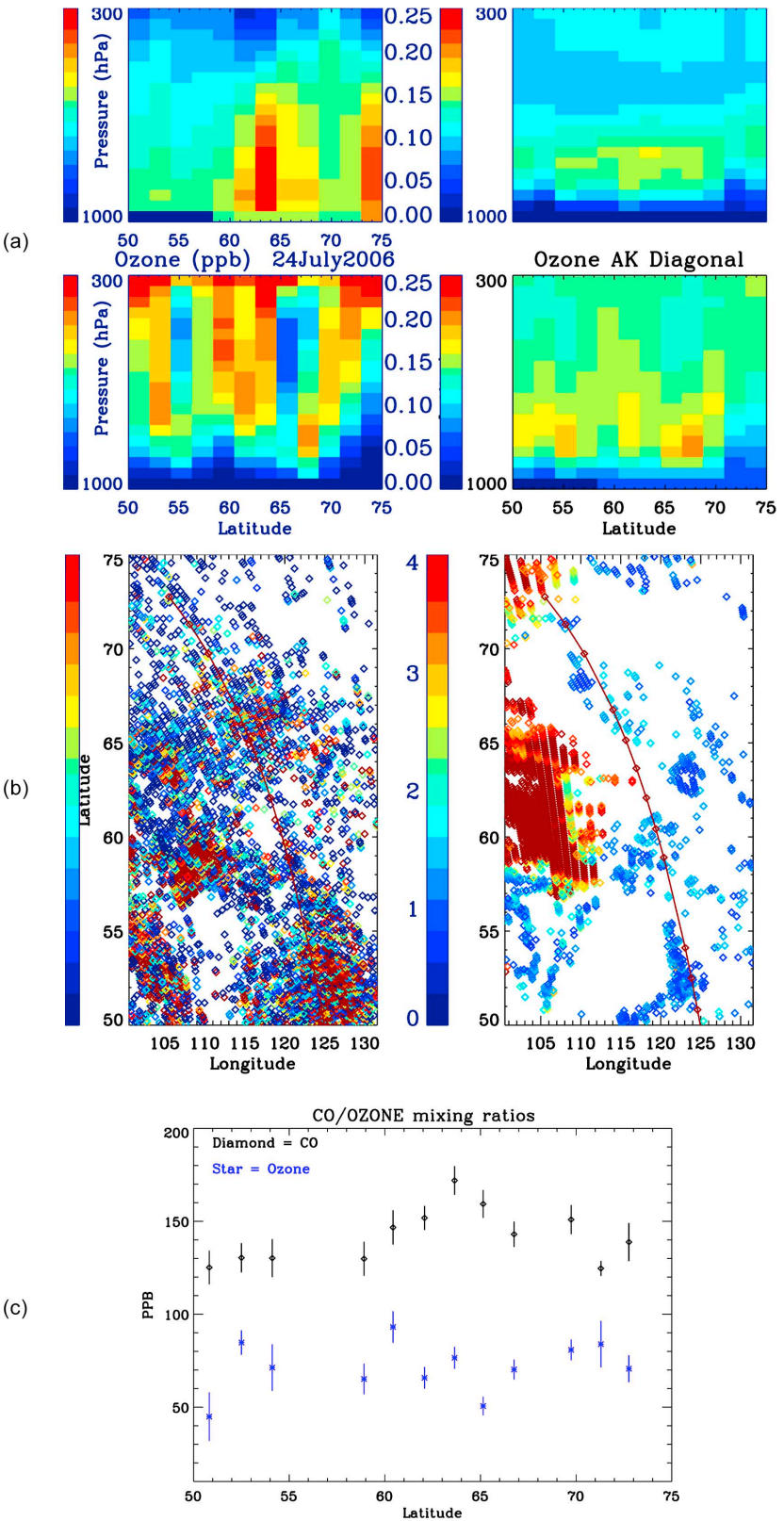
(a)
Pressure (hPa)
300
1000
0.25
0.20
0.15
0.10
0.05
0.00
50 55 60 65 70 75
Ozone (ppb) 24July2006
Ozone AK Diagonal
Latitude
(b)
Latitude
Longitude
75
70
65
60
55
50
105 110 115 120 125 130
4
3
2
1
0
(c)
CO/OZONE mixing ratios
Diamond = CO
Star = Ozone
PPB
200
150
100
50
Latitude

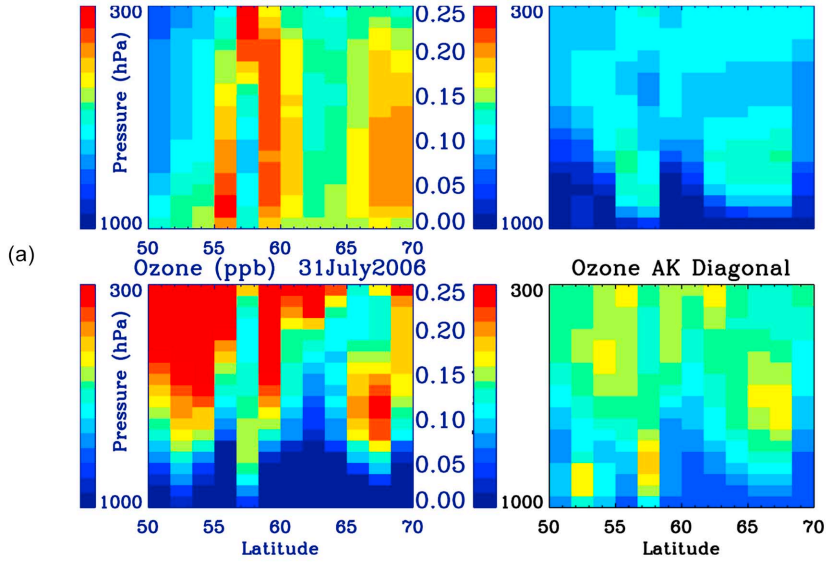
(a)
Ozone (ppb) 31July2006
Pressure (hPa)
300
1000
50
55
60
65
70
0.25
0.20
0.15
0.10
0.05
0.00
Latitude
Ozone AK Diagonal

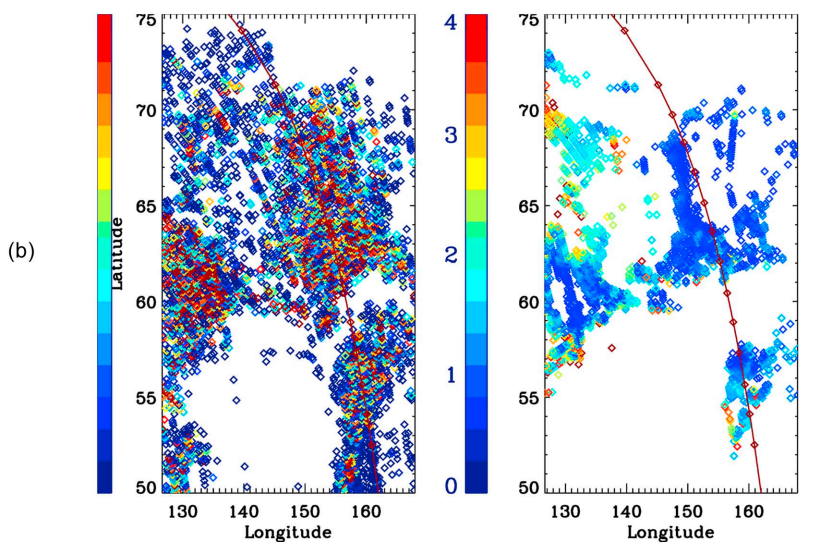
(b)
Latitude
Longitude
75
70
65
60
55
50
130
140
150
160
4
3
2
1
0

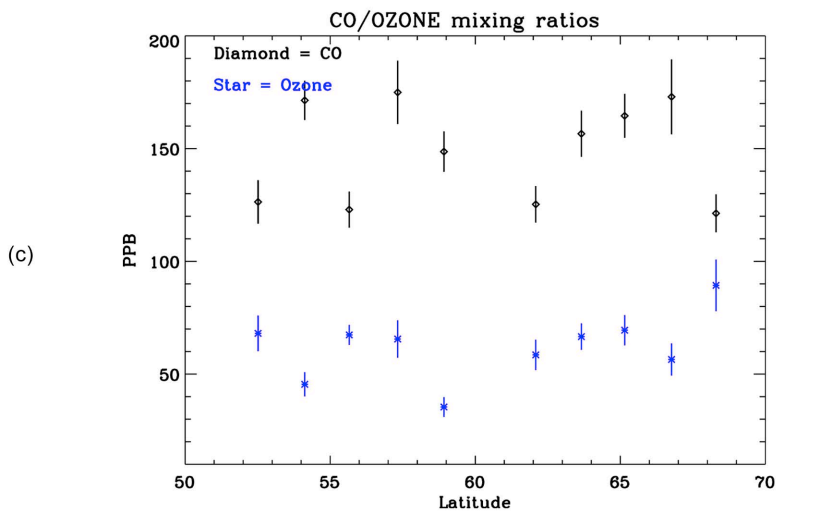
(c)
CO/OZONE mixing ratios
Diamond = CO
Star = Ozone
PPB
200
150
100
50
50
55
60
65
70
Latitude

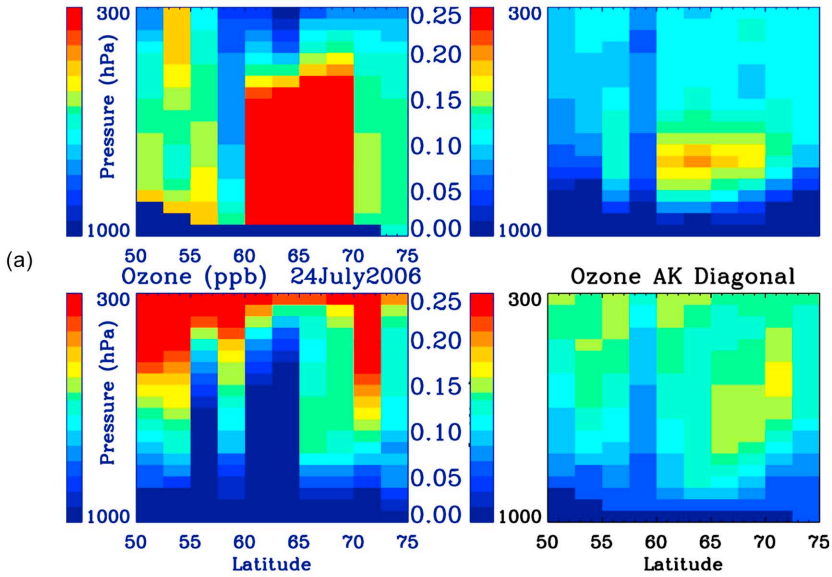
Pressure (hPa)
300
1000
0.25
0.20
0.15
0.10
0.05
0.00
50 55 60 65 70 75
Ozone (ppb) 24July2006
Ozone AK Diagonal
Latitude

(a)

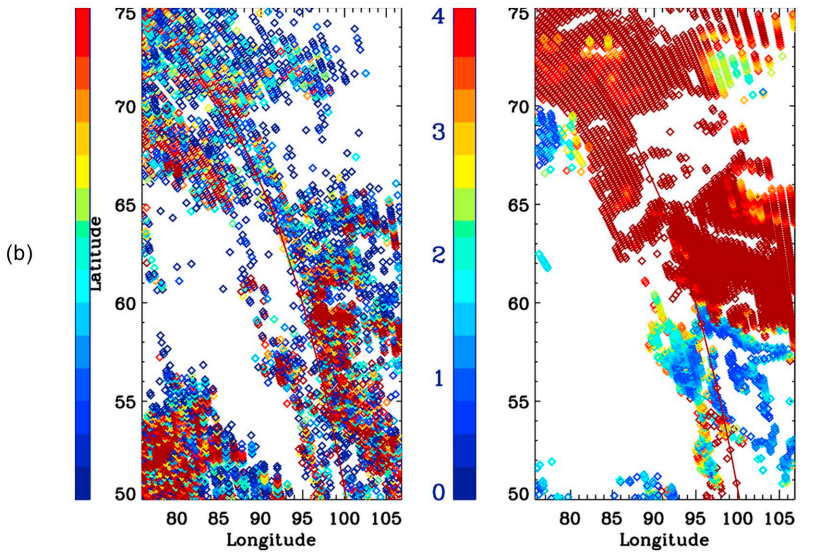
Latitude
75
70
65
60
55
50
4
3
2
1
0
80 85 90 95 100 105
Longitude

(b)

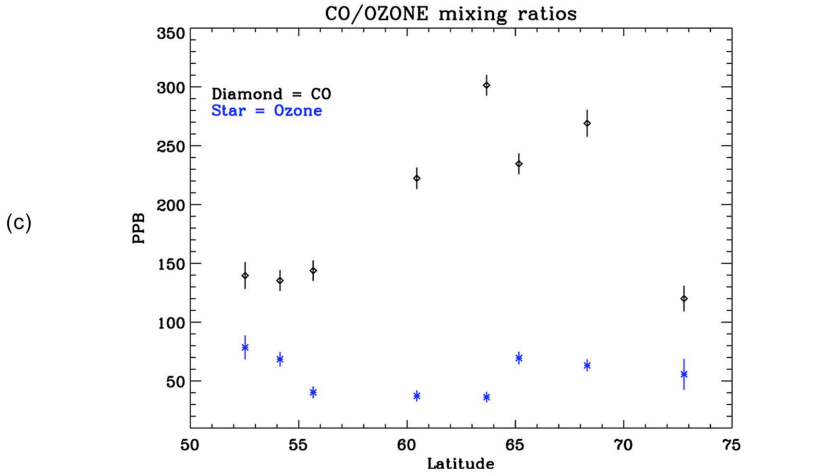
CO/OZONE mixing ratios
Diamond = CO
Star = Ozone
PPB
350
300
250
200
150
100
50
50 55 60 65 70 75
Latitude

(c)

(a)

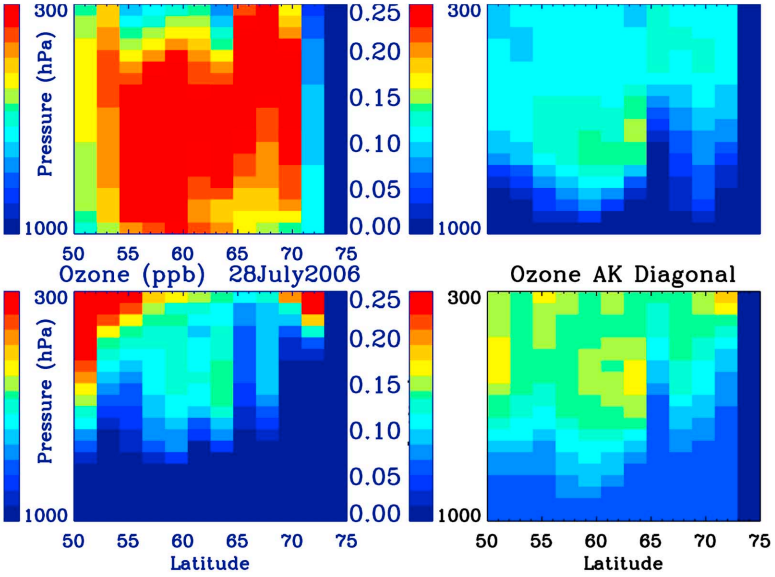
Ozone (ppb) 28July2006
Pressure (hPa)
300
1000
50 55 60 65 70 75
0.25
0.20
0.15
0.10
0.05
0.00
Ozone AK Diagonal
Latitude

(b)

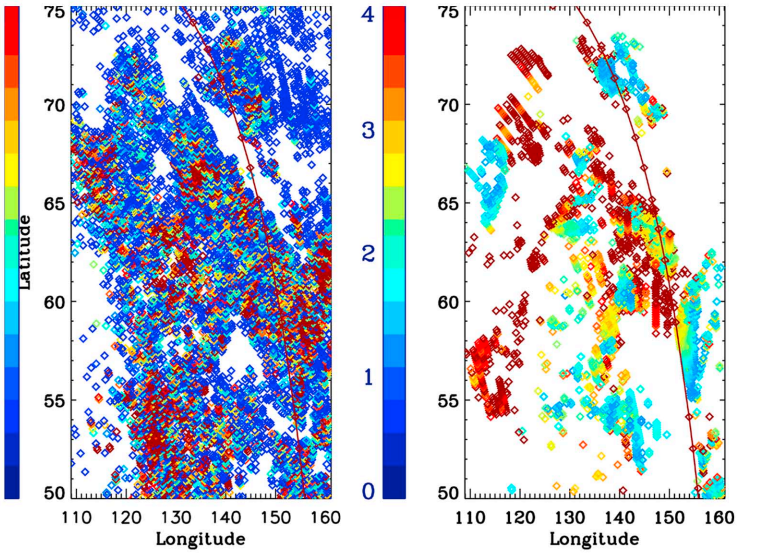
Latitude
75
70
65
60
55
50
110 120 130 140 150 160
Longitude
4
3
2
1
0

(c)

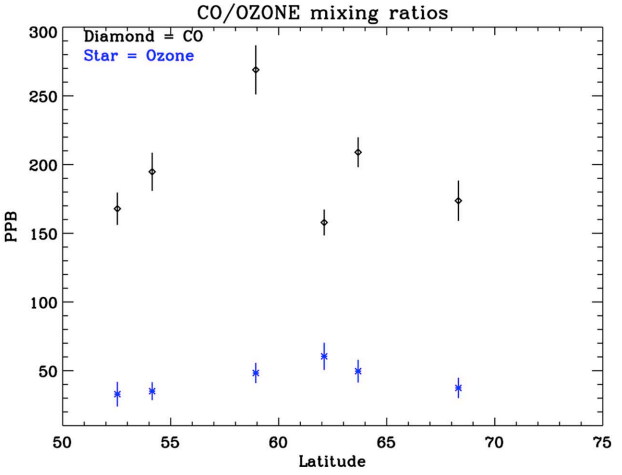
CO/OZONE mixing ratios
Diamond = CO
Star = Ozone
PPB
300
250
200
150
100
50
50 55 60 65 70 75
Latitude

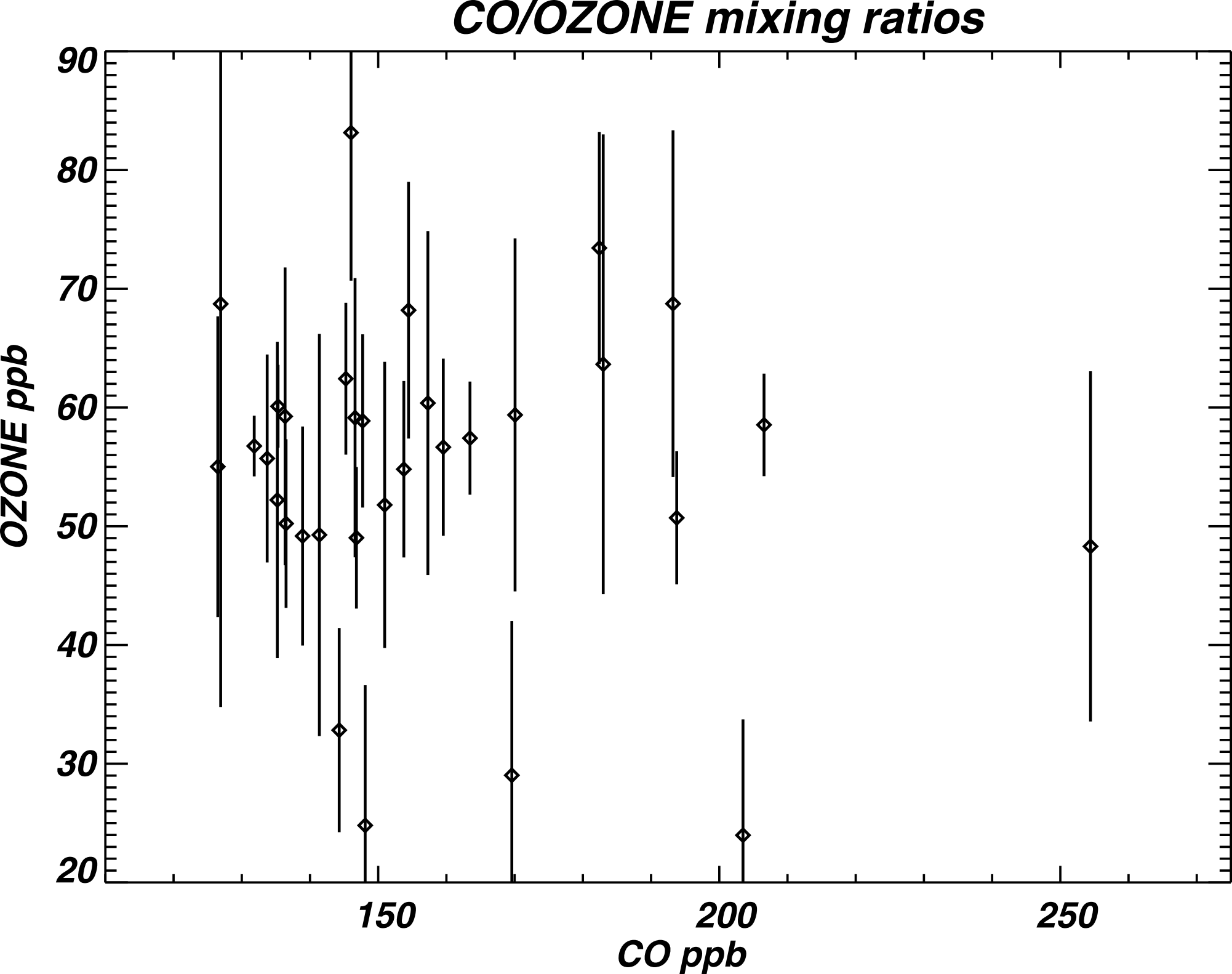
CO/OZONE mixing ratios
OZONE ppb
90
80
70
60
50
40
30
20
150
200
250
CO ppb

(a)

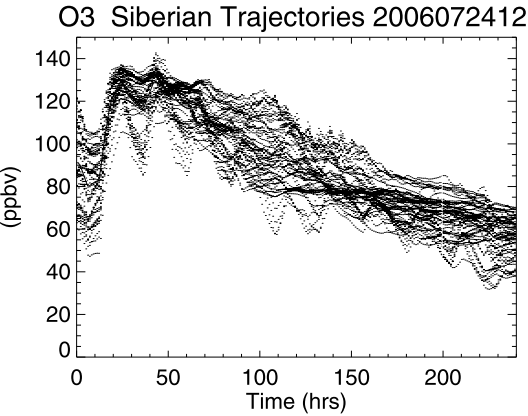
O3 Siberian Trajectories 2006072412
(ppbv)
Time (hrs)

(b)

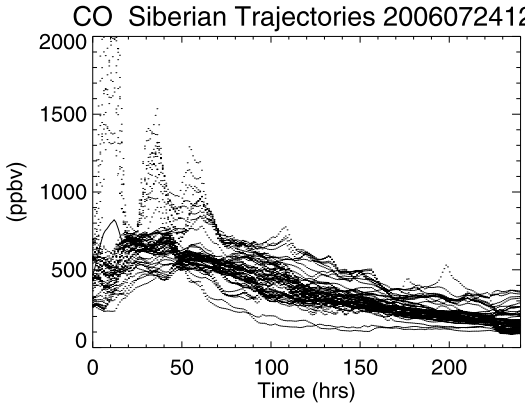
CO Siberian Trajectories 2006072412
(ppbv)
Time (hrs)

(c)

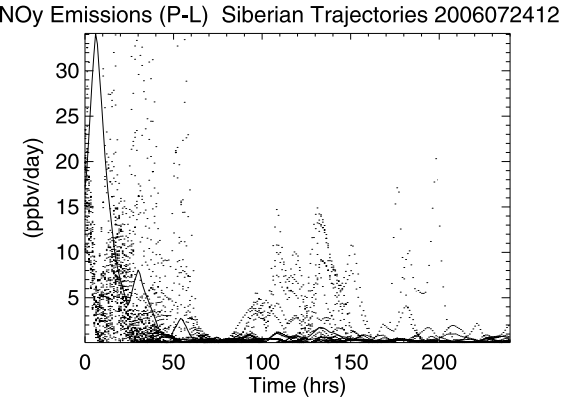
NOy Emissions (P-L) Siberian Trajectories 2006072412
(ppbv/day)
Time (hrs)

(d)

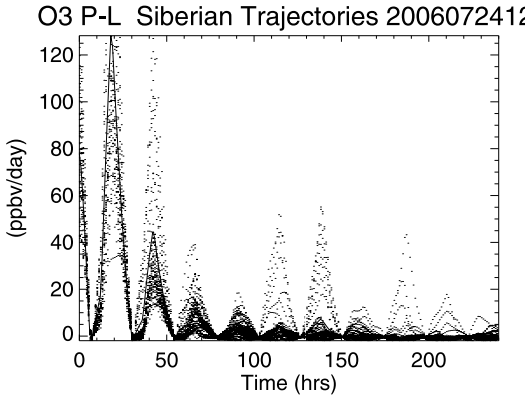
O3 P-L Siberian Trajectories 2006072412
(ppbv/day)
Time (hrs)

(a)

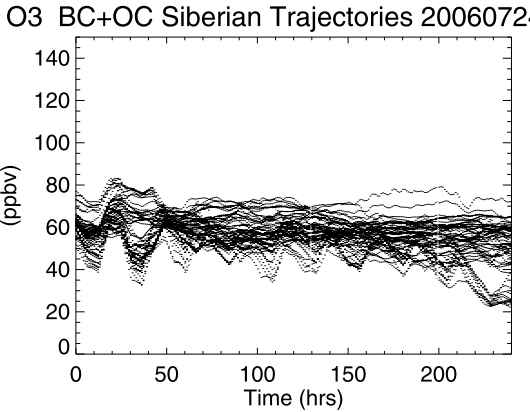
O3 BC+OC Siberian Trajectories 2006072412
(ppbv)
Time (hrs)
0
20
40
60
80
100
120
140
0
50
100
150
200

(b)

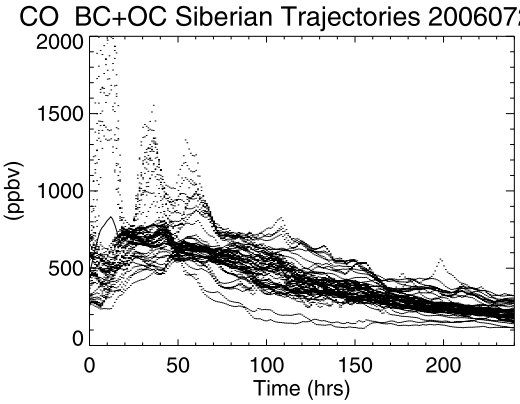
CO BC+OC Siberian Trajectories 2006072412
(ppbv)
Time (hrs)
0
500
1000
1500
2000
0
50
100
150
200

(c)

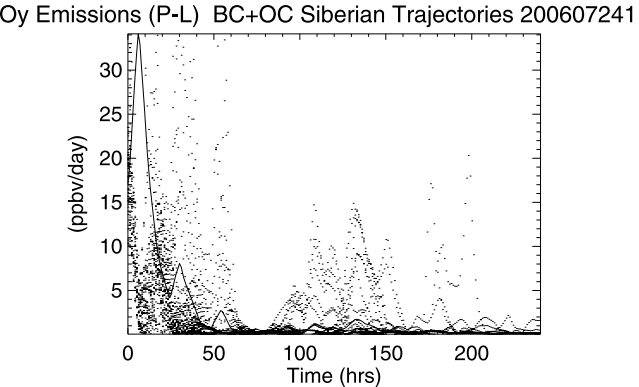
Oy Emissions (P-L) BC+OC Siberian Trajectories 200607241
(ppbv/day)
Time (hrs)
5
10
15
20
25
30
0
50
100
150
200

(d)

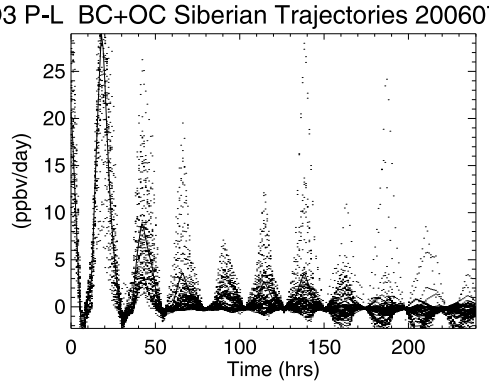
O3 P-L BC+OC Siberian Trajectories 2006072412
(ppbv/day)
Time (hrs)
0
5
10
15
20
25
0
50
100
150
200